Ultrasonics 130 (2023) 106927

Contents lists available at ScienceDirect

Ultrasonics

journal homepage: www.elsevier.com/locate/ultras

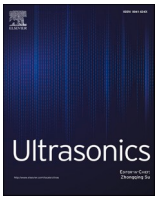

Development and evaluation of a titanium-based planar ultrasonic scalpel for precision surgery

Martin Hofmann [a,f,*], Andreas Haeberlin [b,g,h], Simone de Brot [c], Andreas Stahel [d], Herbert Keppner [e], Juergen Burger [a,i]

[a] School of Biomedical and Precision Engineering, University of Bern, 3008 Bern, Switzerland
[b] Department of Cardiology, Inselspital, Bern University Hospital, University of Bern, 3010 Bern, Switzerland
[c] COMPATH, Institute of Animal Pathology, University of Bern, 3012 Bern, Switzerland
[d] School of Engineering and Computer Science, Bern University of Applied Sciences, 2501 Biel, Switzerland
[e] Haute Ecole Arc Ingénierie, University of Applied Sciences Western Switzerland (HES-SO), 2300 La Chaux-de-Fonds, Switzerland
[f] Graduate School for Cellular and Biomedical Sciences, University of Bern, 3012 Bern, Switzerland
[g] ARTORG Center for Biomedical Engineering Research, University of Bern, 3008 Bern, Switzerland
[h] Swiss Institute for Translational and Entrepreneurial Medicine, 3010 Bern, Switzerland
[i] Department of Orthopaedic Surgery and Traumatology, Inselspital, Bern University Hospital, University of Bern, 3010 Bern, Switzerland

ARTICLE INFO

Keywords:
Ultrasonic scalpel
Ultrasonic surgery
Precision surgery
Piezoelectric transducer
Hemostasis
Equipment design

ABSTRACT

This paper introduces a titanium-based planar ultrasonic microscalpel. The concept of silicon-based planar ultrasonic transducers has already been proven, but they are not yet suitable for clinical use due to material failure. The main objective of this work was to develop a smaller, lighter, and more cost-effective ultrasonic scalpel that could be used as an alternative or supplementary device to current surgical instruments. Various prototypes were fabricated and characterized, differing in bonding by three epoxy adhesives and two solder pastes as well as three variations in tip design. The instruments were designed to operate in the frequency range of commercial instruments and to generate a longitudinal displacement amplitude. The electro-mechanical characterization through impedance analysis and vibration measurements was complemented by an *in vitro* cutting trial and an acute *in vivo* animal experiment in comparison to commercial ultrasonic and electrosurgical devices. The operating frequency was around 40 kHz and 48 kHz depending on whether matched or unmatched operation was used. Unmatched operation turned out to be more suitable, achieving displacement amplitudes of 25.3 µm and associated velocity amplitudes of up to 7.9 m/s at an electrical power of 10.2 W. The cutting ability was demonstrated *in vivo* by successful dissection even under anticoagulation. The geometry of the instrument tip was found to have a major influence on cutting performance by affecting the resonance behaviour and tissue penetration.

1. Introduction

Ultrasonic surgical instruments are gaining in importance in the operating room, as they enable greater control for the surgeon, reduced tissue damage, shortened operating times, and promote faster healing. Ultrasonic instruments are valued for surgical applications as they allow efficient and safe cutting, ablation, and coagulation of biological tissue [1–4]. Ultrasonic cutting instruments are used in a wide range of surgical fields, such as orthopedic, ophthalmic, plastic, oral-maxillofacial, urological, neuro, and other open or endoscopic procedures [5,6]. Ultrasonic dissection devices are mainly intended for soft tissue surgery whenever bleeding control and minimal thermal lesions are desired. Tissue dissection and coagulation are caused by the introduction of longitudinal mechanical vibrations at ultrasonic frequencies ($f > 20$ kHz) leading to longitudinal strain, local heat generation, and cavitation [7–9]. The most important parameters for effective tissue fragmentation are the operating frequency, tissue type, stroke amplitude, and tip shape [9,10]. Therefore, ultrasonic instruments are available as scissors or differently shaped scalpels having simple flat or spherical ends to hooks or curved cutting blades [11,12] and are used as a supplement or alternative to steel scalpels and laser- or electrosurgery. Multiple studies have shown that the outcomes of ultrasonic dissection are associated

* Corresponding author at: Gueterstrasse 24/26, 3008 Bern, Switzerland.
E-mail address: martin.hofmann@unibe.ch (M. Hofmann).

https://doi.org/10.1016/j.ultras.2023.106927
Received 3 May 2022; Received in revised form 21 October 2022; Accepted 4 January 2023
Available online 6 January 2023

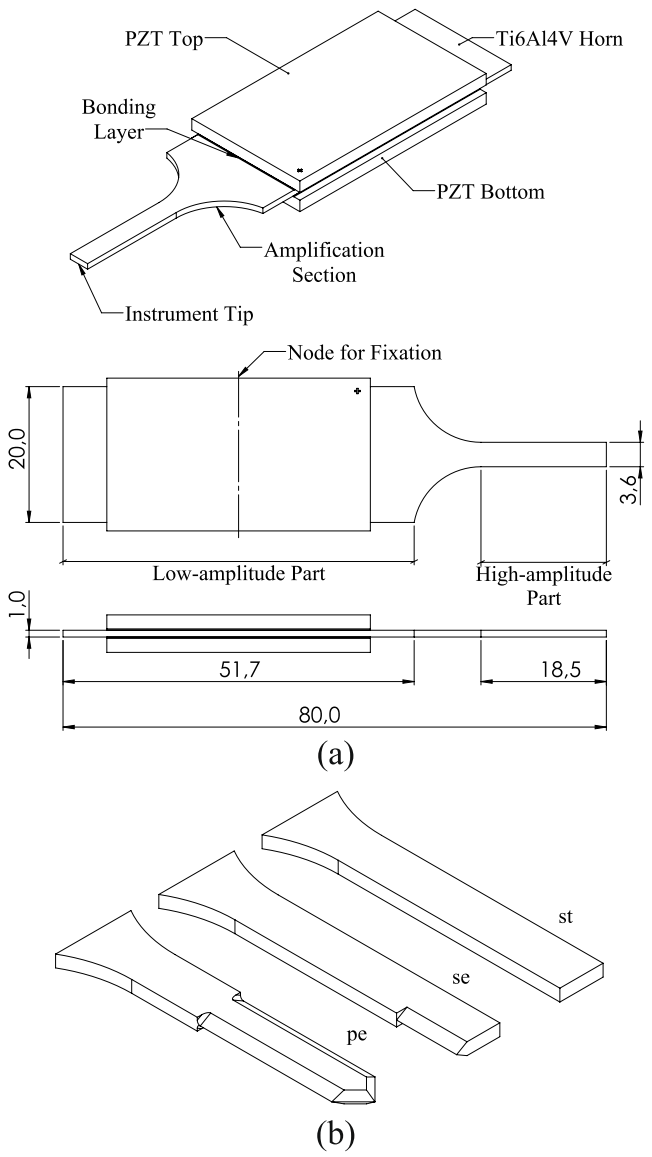

Fig. 1. (a) Design and composition of the planar titanium-based ultrasonic scalpel; (b) three different tip shapes with a pointy (pe), side-edged (se), and straight tip (st).

Table 1
Overview of the different scalpel prototype configuration.

Epoxy Adhesives	Solder Pastes	Tip Modifications
AD295-st	#281-st	AD295-se
AD066-st	#Sn62-st	AD295-pe
GE785-st		

with less tissue damage compared with electrosurgery [13–16]. However, their use is limited to a few fields of intervention due to the size, weight, and cost of the current systems [11,17,18]. This work aims to develop a new generation of ultrasonic microscalpel transducers for precision surgery.

Attempts have already been made for the miniaturization of Langevin transducers for minimally invasive surgical purposes [19]. A target value for the minimum achievable tip displacement of 30 $\mu m_{p\text{-}p}$ (peak-peak) was defined for the miniaturized transducers tuned to a resonance at 45 kHz. The different transducer configurations had a base diameter of 8 mm, a tip diameter of 2.5 mm, and a length of 50 mm to 70 mm. Other research [18,20,21] reported the development of a miniaturized planar ultrasonic scalpel design based on micromachined silicon. In contrast to a standard Langevin transducer [19,22,23] equipped with a stack of piezoelectric discs, piezoelectric plate actuators were used, mounted on both sides of the planar silicon structure and operated in its transverse resonant mode (d_{31}). The vibration of the actuators was coupled to the silicon horn via an adhesive layer and amplified by the transducer geometry. This resulted in a displacement amplitude at the instrument tip of 10–35 μm_p (peak), depending on the scalpel design and the materials used. The resonant frequency (f_r) ranged from 40 to 120 kHz, depending on the operating mode and the length of the transducer. The achieved tip velocities of up to 14.2 m/s [20] were sufficient to cut and coagulate soft tissue [7]. Thus, the feasibility of a planar ultrasonic scalpel has been demonstrated. However, due to material failure caused by the brittleness of silicon [18,20], a new approach based on a titanium scalpel needs to be further investigated.

Although titanium alloys or stainless steels commonly used in commercial devices have lower hardness and a higher acoustic loss compared to silicon [21], they are still suitable for ultrasonic surgical devices due to their robustness, durability, and safety of the instrument. Planar ultrasonic horns [24] and transducers based on stainless steel [25] were investigated for their feasibility, but have been found to achieved lower performance (3.2 m/s, 35 $V_{p\ extrapolated}$, 76 kHz) [25] compared to planar silicon scalpels (8.5 m/s, 35 V_p, 76 kHz) [18]. There is only limited evidence so far whether the planar scalpel concept can also be transferred to a titanium-based instrument. In addition, the conceptual planar scalpels operate at a higher resonant frequency than commercially available devices (i.e. SonoSurg, Olympus, Japan: 23.5/47 kHz; Harmonic Synergy, Ethicon, United States: 55.5 kHz) [7]. Therefore, the focus of this work is on the evaluation of a titanium-based planar ultrasonic scalpel that is comparable to commercial devices.

2. Materials and methods

2.1. Design and material

For the design of a planar d_{31} mode ultrasonic scalpel, various design parameters had to be examined which influence the performance, efficiency, and robustness of the device. These design parameters included the shape, dimension, and material of the amplifying horn and instrument tip, the type, dimensions, and mounting position of the piezoelectric actuator, and finally the adhesive material and manufacturing process.

The aim was to develop a transducer design that could be operated in both matched half wavelength ($\lambda/2$) mode, where the f_r of the transducer is matched to the d_{31} resonant mode of the piezoelectric plate, and unmatched full wavelength (λ) mode [18]. In matched mode, the piezoelectric actuators are subjected to large deflections due to self-resonance and should be more resistant to damping from external loading [18]. In unmatched mode, the transducer is expected to be easier to control [18]. The same planar transducer configuration introduced by Lal et al. [20] and further developed by Lockhart et al. [18] was used and modified using finite element (FE) simulation (Comsol Multiphysics v. 6.0, COMSOL AB, Sweden). A modified stepped shape [18] with a radius (10 mm) in the transition region was chosen for the horn design (Fig. 1a). This design provides a sufficiently large surface for symmetrical bonding of the lead zirconate titanate (PZT) piezoelectric plates on the low amplitude part and reduces stress concentration at the edges while maintaining a high displacement amplification. The PZT plates were centered on the low amplitude part so that the nodal point (zero displacement) was located in the middle of the PZT (Fig. 1a). As the shape of the probe tip has a direct and significant effect on tip–tissue interaction [8,12], different planar tip shapes were investigated. Besides a straight tip (st), two other designs were chosen with a pointy (pe) and side-edged (se) tip, both with a chamfer of 60° (Fig. 1b). The modified tip designs featured a sharp edge on the cutting side, enhancing precise

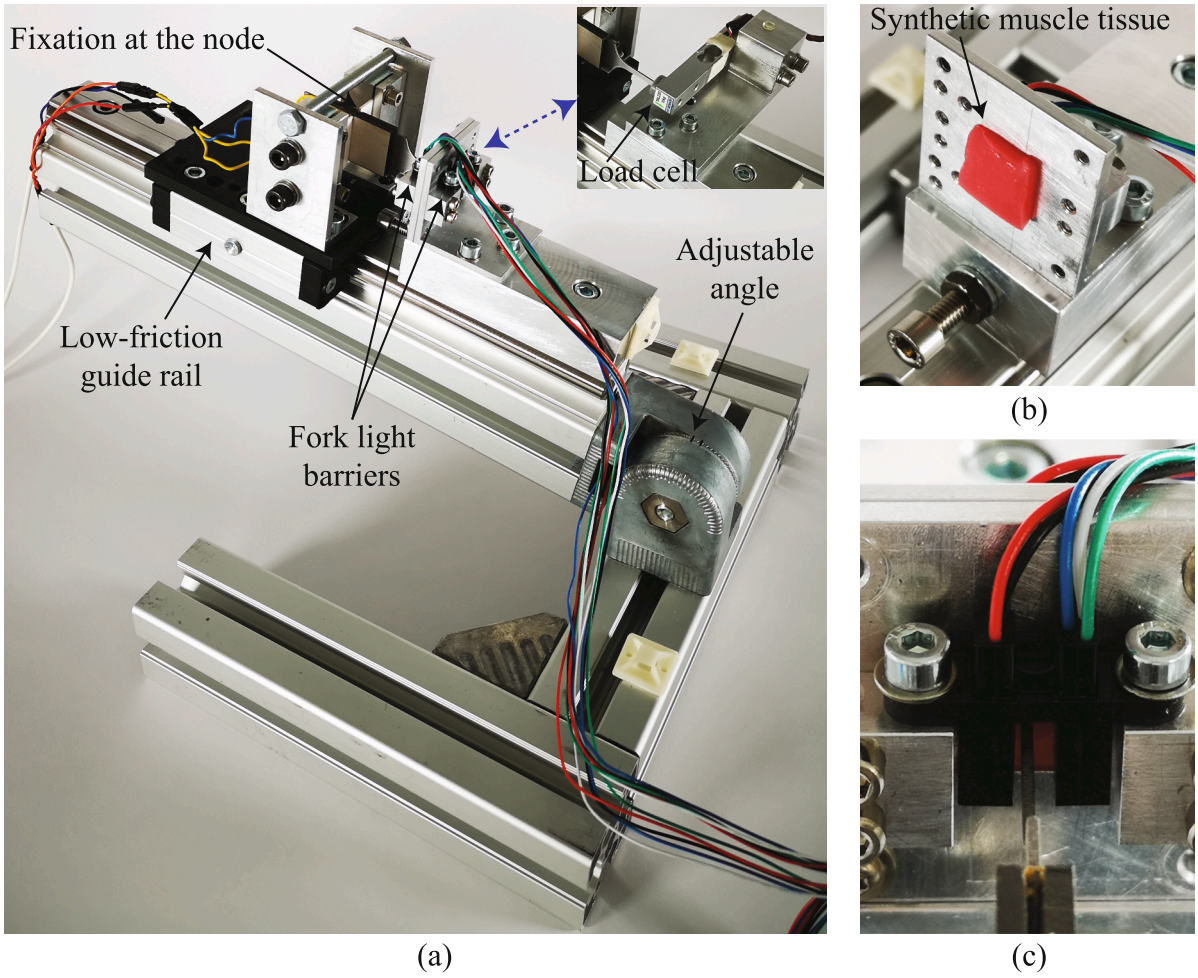

Fig. 2. Test bench for standardized evaluation of the cutting ability; (a) prototype fixed at its node and mounted on a low-friction guide rail with adjustable angle to set the desired effective force. Time measuring unit with two fork light barriers and force measuring unit with a load cell are interchangeable; (b) sample of synthetic muscle tissue positioned in the fixture between the light barriers; (c) assembled timing unit with scalpel cutting through the tissue.

operation. It was supposed that with the asymmetric design (se) a higher total stroke could be achieved due to the additional bending motion [12], while the additional stress should remain low. Moreover, it was reported that by reducing the size of the cutting area, heating caused by friction between the tip and bone tissue is reduced [26], suggesting that the formation of necrosis could also be reduced when cutting soft tissue. The FE model was used to investigate the resonance modes for their longitudinal behaviour and predict the resonance frequencies, vibration amplitudes, and stress distribution. The design was adjusted to have an unmatched longitudinal λ resonant mode at 48 kHz (st). By modifying the tip shape, the resonant frequency was slightly increased, but is still within the range of commercial devices.

A hard PZT-8 material (PIC 181, PI Ceramic, Germany) was chosen due to its high mechanical quality factor ($Q_{m\ datasheet}$: 2000, $Q_{m\ d31\ measured}$: 1355), Curie temperature (T_c: 330 °C) and low dielectric loss (tan δ: 0.003) making it suitable for high-power resonance applications [18,19]. Sadiq et al. [25] have reported that ferroelectric single crystal material could drive planar ultrasonic tools. Although PMN-PT or PZN-PT offer up to ten times higher charge coefficients and higher coupling factors, they are of limited applicability for high-power resonant operation due to the low quality factor, Curie temperature, and stress resistance as well as higher losses and thermal hysteresis [27,28]. The selected PZT plates measured 38.8 mm × 22.5 mm × 2.0 mm and featured fired silver electrodes of 30 µm thickness. As a result of these dimensions, the matched mode was around 40 kHz. The titanium alloy Ti6Al4V grade 5 (AMS 4911) was chosen for this work because it is commonly used for ultrasonic instruments and was also applied by Li et al. [19] to miniaturize Langevin transducers for surgical purpose. Besides its biocompatibility, high strength, and resistance to fracture, it offers the advantages of heat treatability so that the alloy can be adapted to specific requirements [29]. Other materials commonly used in transducer design are stainless steel or high-strength aluminium alloys. The mechanical properties of alternative materials can be found in Table 4 in the appendix. Although steel offers higher stiffness, acoustic transmission is lower than with Ti64 due to its higher density. Aluminium has a lower density, but also a lower tensile strength and the oxidised surface is likely to crack in ultrasonic operation, causing it to lose its inert properties (Al_2O_3 layer) and making it unsuitable for interaction with biological tissue.

2.2. Fabrication

Seven working prototypes were produced, differing in three adhesives, two solder pastes, and three tip shapes (Table 1). The mechanical processing of the titanium horns and PZT plates was performed by water jet cutting, as this process is suitable for heat-sensitive materials. Optimal cutting parameters for the piezoceramics had to be evaluated in a preliminary experiment to prevent microcrack formation. Machining with a pressure of 3600 bar, a cutting speed of 5 mm/min, and 300 g of abrasive garnet sand achieved good results in that the piezoceramics did

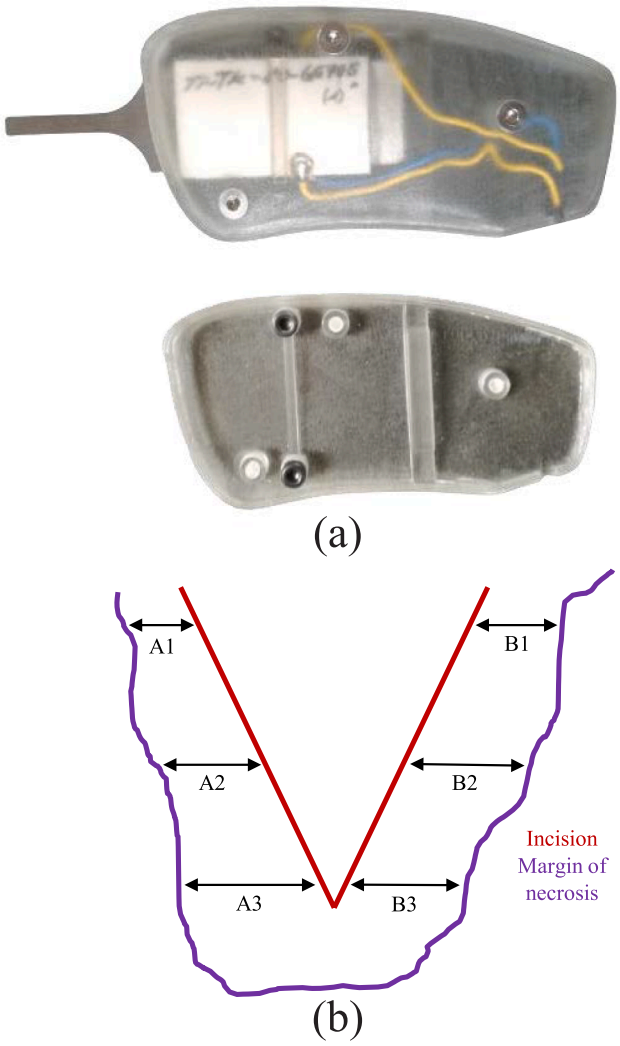

Fig. 3. (a) Manufactured microscalpel prototype (GE785-st) integrated in a housing. The transducer is fixed at the node with a screwed compression bridge; (b) illustration of the cross section of the incised muscular tissue, indicating the performed histologic measurements of the lateral extent of necrosis. Measurements were performed separately for each lateral side (A, B), at three different levels (1: apical, 2: middle, 3: deep).

not break at the edges and retained their piezoelectric properties. The tip designs were shaped in an additional milling process. A suitable pretreatment of the surfaces was necessary for optimum adhesion of the subsequent bonding. This included sanding with 600-grain size to remove the oxide layer and increasing the adhesion by improving the roughness, followed by various ultrasonic cleaning processes using alkaline cleaning agents and solvents. In the soldering process, the wettability and adhesion and, thus, the solderability are considerably affected by the oxide layer coating the titanium part. Therefore, to obtain a good solder joint, a 4 μm copper layer was applied to the polished titanium horn (#281-st, #Sn62-st) using RF magnetron sputtering technology. For the adhesive bonding, the preselected epoxy types were applied by stencil printing with a layer thickness of 200 μm and subsequently cured in a vacuum oven at 150 °C for 20 min. The solder pastes were processed according to a reflow sequence with parameters provided by the manufacturer. To electrically contact the electrodes, wires were soldered to the silver-plated PZT surfaces. For the cutting tests, the fabricated transducers were integrated into a 3D-printed prototype housing (Object 30 Prime with RGD720, Stratasys, Israel) and mechanically fixed to the node with a 2 mm wide compression bridge (Fig. 3a).

2.3. Electro-mechanical characterization

Both electrical and mechanical tests were conducted to characterize the transducer prototypes and examine their performance in resonant operation. The relevant resonant modes, matched $\lambda/2$ and unmatched λ, were identified by electric impedance magnitude and phase measurements ($P < 0.2$ W: MFIA, Zurich Instruments, Switzerland; $P > 0.2$ W: TA189 current probe, Pico Technology Ltd., United Kingdom). These parameters are essential for assessing the controllability of the transducer in resonance. The achievable velocity amplitudes of the tip center, used as a mechanical performance indicator, was measured using a laser Doppler vibrometer (PSV 300, Polytec, Germany). The prototypes were operated with two parallel connected A-303 high voltage amplifiers (A. A. Lab-Systems, Israel) with a sinusoidal signal at a voltage of up to 40 V_p and the tip deflection was recorded in a frequency range of 30–50 kHz. In this configuration, the peak current was limited to 450 mA and defined the maximum operating conditions. Additional measurements at tracked resonance (zero phase tracking) were performed for both, matched and unmatched modes (40 kHz, 48 kHz) at electrical power levels up to 12 W. The force factor A_{31}, representing the ratio between electrical current and the mechanical velocity amplitude [30], was used in its inverse form ($A_{31}^{-1} = v/I$) to evaluate the electro-mechanical characteristics of the prototypes as it directly represents the overall system performance, including the electric driver. Additionally, the mechanical quality factor, which characterizes the behaviour at resonance, was analyzed using the 3 dB method applied to the velocity measurements.

2.4. Temperature monitoring

Thermal losses are caused by the dielectric losses of the PZT, the internal friction in the adhesive layer and, in loaded operation, by the friction at the scalpel tip. Excessive heating can lead to uncomfortable handling of the device or even material failure. Therefore, an infrared camera (FLIR A655sc, Teledyne FLIR LLC, United States) was used to measure the heat development during operation. For thermography, the emissivity of the different materials is of importance. For this reason, all components of the prototype AD066-st were dyed black (Dupli Color RAL 9005, European Aerosols GmbH, Germany). A calibration at 23 °C and 45 °C resulted in an emissivity of $\varepsilon = 0.94$ for all components. The temperatures of the titanium horn, PZT plate and a wire were monitored (Fig. 9). Additionally, a type K thermocouple (T012.0,20.1K.02000, Roth + Co, Switzerland) was used to measure a reference temperature between the two piezoceramic plates close to the soldering spot. A thermal paste based on synthetic silver (Arctic Silver 5, Arctic Silver, Inc., United States) was used to increase the thermal conductivity. As it was not practical to measure the temperature during the continuous cutting of soft tissue, two separate measurements were carried out: an unloaded measurement over 2 min and an extremely loaded measurement with a rigid load over 10 min.

2.5. Operational tests

Since the microscalpel is intended for soft tissue dissection in open surgery, its cutting ability is the main measure to be assessed. Two separate tests were performed to evaluate the cutting ability of muscle and skin tissue. The choice of tissue was based on the requirement of a sufficiently large area with the same or very similar properties for the various incisions. Although healthy muscle tissue should always be preserved, in certain procedures it must be removed for reconstruction, accessibility or due to adhesions. An example of such a procedure using the harmonic scalpel is the flap dissection in reconstructive head and neck surgery [13,31].

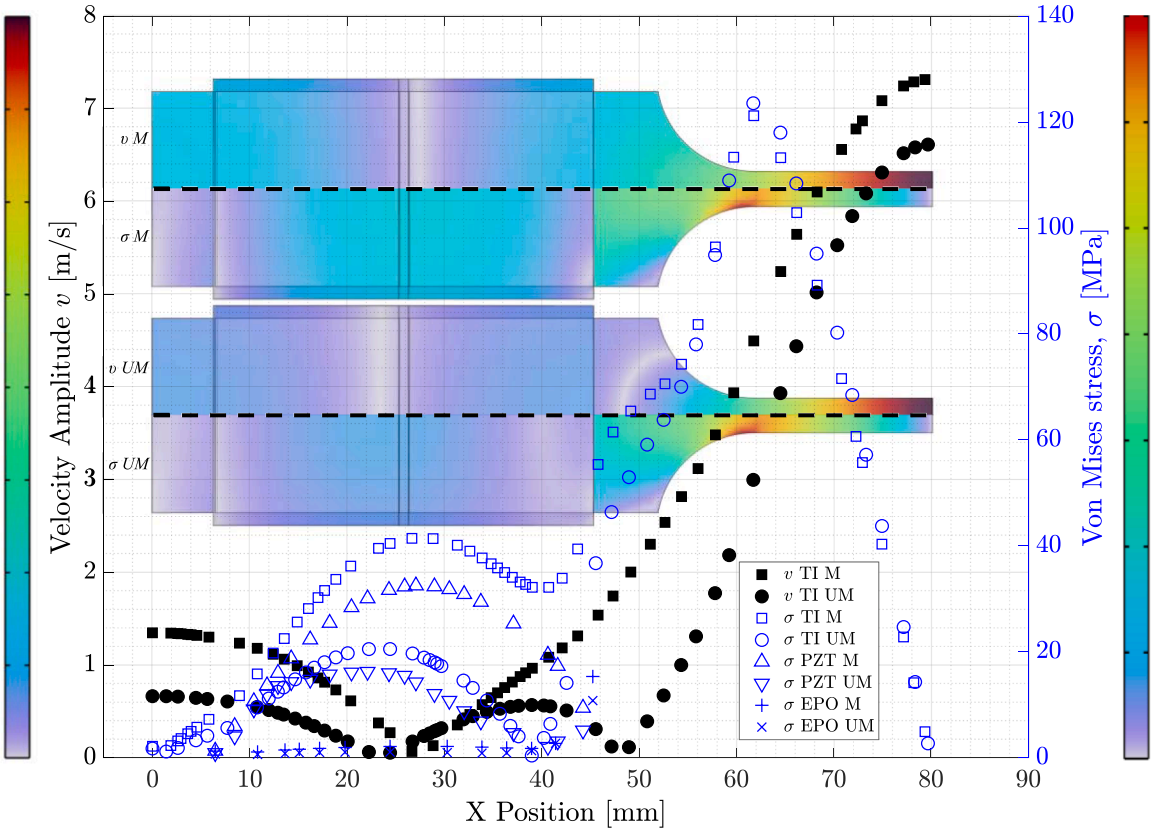

Fig. 4. Velocity amplitude (left) and Mises peak stress (right) of the simulation model (st) determined on the center line (dashed) at 20 V_p for matched (M) and unmatched (UM) mode. Evaluation for horn (TI), top piezo ceramic (PZT), and adhesive layer (EPO). Markers represent every tenth simulation point. The upper half of the surface plots indicates the velocity, and the lower half the stress.

2.5.1. *Standardized cutting test*

To characterize the cutting ability in a standardized setting, a test bench was developed to quantify the time required for linear tissue separation (Fig. 2). The scalpel prototypes were placed in a metal bracket mounted on a low-friction guide rail with variable angle position. The actuating force resulting from the adjustable position was measured using a load cell (TAL 220, HT Sensor Technology Co., China). The load cell was pre-calibrated with weights of 10 g and 100 g and showed an error of less than 1 %. A force of 1.5 N proved to be sufficient in a cutting test with a commercial ultrasonic scalpel (Harmonic Synergy SNGCB, Ethicon, United States) and is consistent with previously reported values [18,32]. A sample of synthetic muscle tissue (skeletal muscle tissue plate, SynDaver Labs, United States) measuring 20 mm × 20 mm × 5 mm was fitted into a fixture (Fig. 2b). The tissue thickness could be doubled by using two samples. Timing was triggered and terminated by fork light barriers positioned in front of and behind the fixture (Fig. 2c). A commercial amplifier with a frequency matching function (Gen 300, Ethicon, United States) was used to operate the prototypes at their resonant frequencies. The tests were performed three times for all prototypes at both matched and unmatched resonances for tissue thicknesses of 5 and 10 mm. The time measurement between the two light barriers was accurate to 100 ms.

2.5.2. *Animal trial*

To investigate the effect and efficiency of the different prototypes when applied to biological tissue, the prototypes were evaluated in an acute *in vivo* trial. In an animal experiment (white domestic pig, 70 kg), three microscalpel prototypes (AD295-st/pe/se), which differ in the geometry of the tip, were compared to a standard steel scalpel, a commercial ultrasonic scalpel (Harmonic Synergy SNGCB, 55 kHz, Ethicon, United States), and an electrosurgical instrument, monopolar 350 kHz, 60 W (ARC 400 and ErgoPEN 2.4 mm, BOWA-electronic GmbH & Co., Germany). The use of these additional reference instruments was intended to provide additional data for the comparison of electrosurgery with ultrasonic surgery. The experiment received approval from Veterinary Department of the Canton of Berne, Switzerland. The prototypes were operated with the commercial Gen 300 amplifier in unmatched λ mode (48 kHz), while the most promising prototype (AD295-pe) was additionally operated in matched λ/2 mode (40 kHz). Prior to the trial, an electro-mechanical characterization at constant resonant frequency and a cutting test was carried out to exclude significant changes in performance due to the prototype housing. Incisions were performed in the epidermis/dermis and the trapezius muscle along the direction of the muscle fiber and time was measured to achieve cuts approximately 20 mm in length and 5 mm in depth. For each defined trial set, three incisions were performed per prototype. Furthermore, additional incisions were performed with heparin supplementation (ACT: 513 s), allowing the coagulation effect to be demonstrated more effectively under enhanced bleeding [33]. An acute and extended (3 h) coagulation effect study was performed by visually monitoring the post-cut bleeding, cleaning with medical swabs, and measuring the hemorrhage time. Subsequently, the cutting sections were explanted and fixed in buffered formalin (4 %) for histological examination.

2.6. *Histological examination*

A total of n = 12 formalin-fixed porcine muscular (n = 9) and skin (n = 3) tissue fragments, corresponding to Group A-L, were examined by a board-certified veterinary pathologist. Each tissue fragment included three macroscopically visible incisions. Of each incision, one cross-

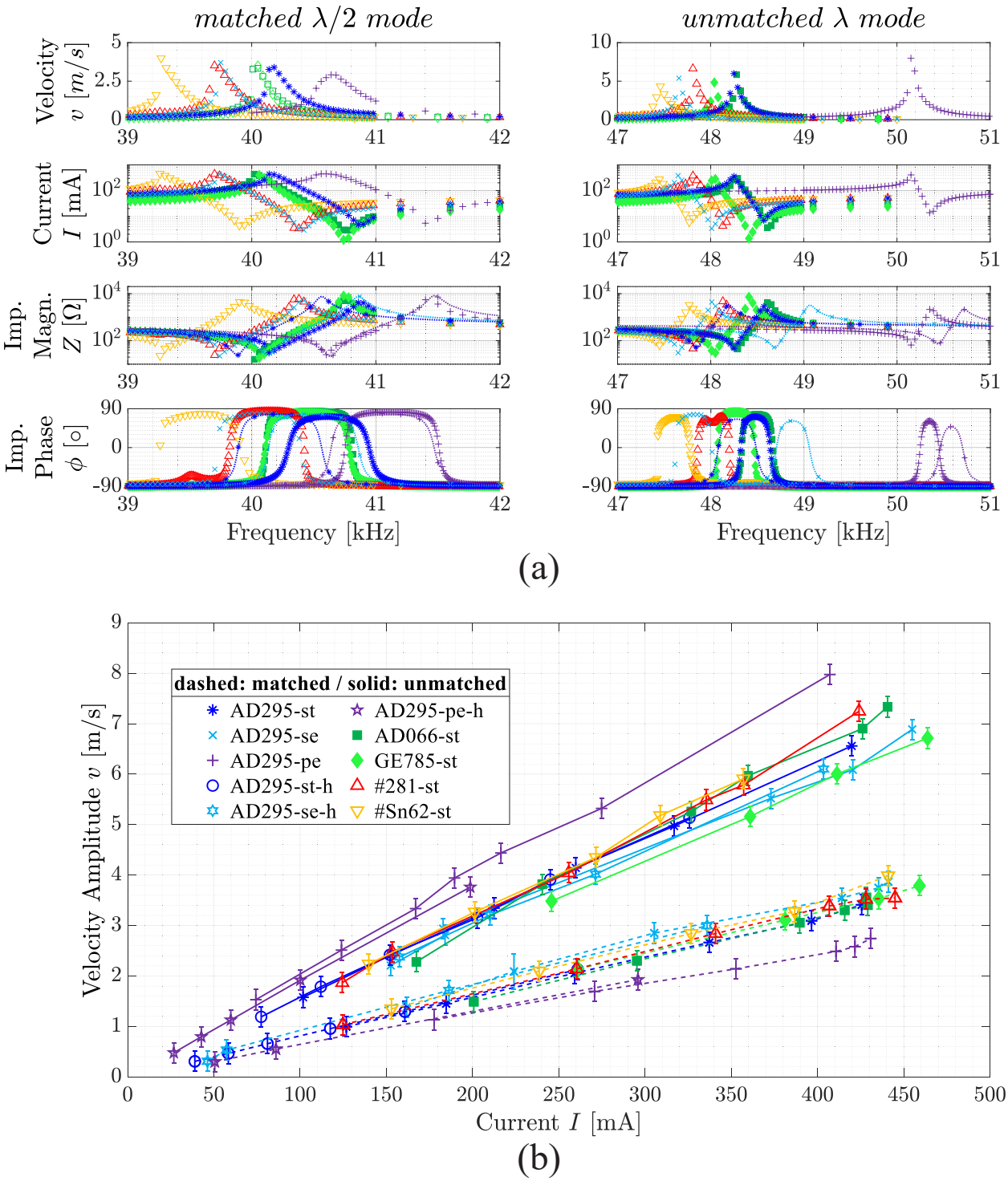

Fig. 5. (a) Electro-mechanical characterization of all prototypes in the range of both matched and unmatched modes with a maximum current in unmatched mode of about 400 mA ± 10 %. Markers represent every third measuring point. The simulation results for the AD295 prototypes are indicated by the dotted lines; (b) mechanical vibration measurement at resonance in function of the current (inverse force factor A_{31}^{-1}). Label h indicates measurements on prototypes in a housing.

section and two longitudinal sections were trimmed, which were routinely processed for histological examination by staining with hematoxylin and eosin (H&E). The lateral extent of necrosis was measured digitally on the cross-section of the incision on three different levels (apical, middle, deep third of the incision) on each side, as indicated in Fig. 3b. This was done by drawing digital horizontal lines from the incision to the margin of tissue necrosis. For statistical purpose, a Friedman test was performed for the different groups (A-L) and instrument types (A-D, F, L), and a Mann-Whitney *U* test was applied for the different tissue types (F-K). Inflammatory changes were further assessed in a semi-quantitative approach for the following parameters: Severity (0: absent, 1: mild, 2: moderate, 3: severe), predominant type of leukocyte, and distribution (focal vs. multifocal; relevant association with muscular vs. non-muscular tissue, tissue necrosis, blood vessels and incision).

Table 2
Series resonant frequencies f_r and corresponding minimum impedance values Z_r, and mechanical quality factor Q_m (for I: 400 mA) as well as inverse force factor A_{31}^{-1} values of all prototypes for matched λ/2 (M) and unmatched λ (UM) mode. Cutting test: evaluation of the linear cutting ability by measuring the mean penetration time [s] for 5 mm and 10 mm synthetic tissue thickness. INF: failed to penetrate tissue. Measurement error < 10 %. * Due to the asymmetric behaviour, the 3 dB method is only of limited validity.

	f_r [kHz]		Z_r [Ω]		Q_m [-]		A_{31}^{-1} [m/s/A]		Cutting test 5 mm [s]		Cutting test 10 mm [s]	
	M	UM	M	UM	M*	UM	M	UM	M	UM	M	UM
AD295-st	40.2	48.2	29	39	264	846	8.0	15.6	12.1	2.1	INF	3.8
AD295-se	39.7	47.6	21	27	393	867	8.8	15.1	6.9	2.1	INF	3.5
AD295-pe	40.7	50.2	25	65	140	783	6.4	19.4	4.3	1.1	5.6	1.8
AD066-st	40.0	48.3	16	23	336	846	8.3	16.6	11.1	5.3	INF	7.2
GE785-st	40.0	48.0	12	17	519	1263	8.5	15.4	8.2	2.4	INF	11.7
#281-st	39.7	47.8	20	37	265	1062	7.8	17.1	7.3	2.5	INF	3.8
#SN62-st	39.3	47.4	23	47	393	1129	9.1	16.6	7.6	2.6	INF	3.5

Table 3
Labelling, required cutting time, and histological examination of n = 12 (Group A to L) muscle and skin tissue fragments. Elec: Electrosurgery ErgoPEN, Stan: Standard steel scalpel, Syn: Harmonic Synergy, M. trap.: Musculus trapezius, ACT: Activated coagulation time, NecLat: Lateral necrosis, IQR: Interquartile range.

Instrument	**AD295-pe**	**Syn**	**AD295-st**	**AD295-se**	**AD295-pe**	**Elec**	**Syn**	**Syn**	**AD295-pe**	**Elec**	**AD295-pe**	**Stan**
Group	A	B	C	D	E	F	G	H	I	J	K	L
Frequency [kHz]	48	55	48	48	40	350	55	55	48	350	48	–
Tissue	M. trap.	M. trap.	M. trap.	M. trap.	M. trap.	M. trap.	Skin	M. trap.	Skin	Skin	M. trap.	M. trap.
ACT [s]	–	–	–	–	–	513	513	513	513	513	513	–
Median (IQR) Cutting Time [s]	32 (9)	12 (2)	48 (12)	31 (14)	52 (5.5)	3 (0.5)	10 (3.5)	8 (0.5)	26 (5)	2 (0.5)	11 (0.5)	11 (1)
Median (IQR) NecLat [μm]	1282 (551)	952 (513)	229 (1692)	1143 (519)	403 (138)	105 (149)	808 (676)	1150 (540)	2096 (489)	673 (233)	971 (315)	159 (160)

3. Results

3.1. Finite element simulation

A 3D multiphysics FE model was created for the AD295-st configuration and adapted for the tip modifications (se, pe). The simulation was adapted to the measured electrical impedance amplitude using Rayleigh damping (Fig. 5a). Both modes, matched λ/2 and unmatched λ, were analysed regarding mode shape, mechanical vibration and resulting stresses (Fig. 4). The matched mode has a node slightly in front of the PZT centreline. The unmatched mode has two nodes, whereby the one close to the PZT centre is shifted backwards by about 4 mm and a second, radial node is located in the amplification section. The stress analysis provided peak values after the amplification section of about 120 MPa (at 20 V_p), independent of the resonant mode. In matched mode, however, the stresses in the PZT were higher with a peak value of 33 MPa at the node. The simulation indicated that a higher tip velocity is reached in matched mode although f_r is lower. However, the simulation did not account for the non-linear behaviour of the PZT, dominating the matched mode, and therefore only applies to a limited extent at higher power. Examination of the tip designs indicated that the side edge tip (se) had a slight displacement in the Y-direction due to the asymmetric design and the lack of a compensating mass, but this only accounted for about 3 % of the longitudinal displacement (Fig. 8). For the symmetrical tips (st, pe), the non-longitudinal components were less than 1 %.

3.2. Electro-mechanical characterization

Electric impedance and mechanical vibration measurements were carried out on all prototypes in a voltage range from 1 V_p to 40 V_p. The data were acquired for frequencies between 30 and 52 kHz with an increment of 100 Hz and 10 Hz around the resonances ($f_r \pm 1$ kHz). The electrical series resonant frequency, where minimal impedance magnitude (Z_r), the current peak, and phase zero-crossing occur, coincided with the mechanical resonance, where the maximum vibration amplitude was reached (Fig. 5a). The velocity of the transducer tip was linearly proportional to the electric current for all prototypes, whereby a lower slope (A_{31}^{-1}) could be determined for the matched mode (Fig. 5b). No significant differences were observed when operating in a housing (label h), indicating that the prototypes were correctly fixed to their node. In unmatched mode, the highest A_{31}^{-1} value was achieved by AD295-pe (19.4 m/s/A). Further, AD066-st and the soldered prototypes (#281-st, #SN62-st) achieved slightly higher A_{31}^{-1} values compared to the AD295 adhesive (Fig. 5b, Table 2). The resonant frequencies of the prototypes ranged from 39.3 kHz (#SN62-st) to 40.7 kHz (AD295-pe) for the matched and from 47.4 kHz to 50.2 kHz for the unmatched mode (Table 2). Although Z_r is lower for the matched mode, the quality factor is worse compared to the unmatched mode (Table 2). Further, the quality factors at unmatched resonance tended to be higher for prototypes with a stiffer composite (Table 5). All prototypes exhibited an impedance phase shift of > 90° at both resonances and therefore a phase zero-crossing (Fig. 5a), which is an important factor for resonance tracking. The prototypes were operated up to a power of 12 W. No significant increase in electrical power was observed between free operation and soft tissue cutting. Also, no excessive heat development was detected in unloaded operation (38 °C, 120 s) and the prototypes still function properly even after continuous operation of 10 min under extreme conditions (Fig. 9). The weight of the prototypes, without housing, is 36 g ± 1 g. The best results were obtained with the prototype AD295-pe. At the unmatched λ resonant frequency of 50.2 kHz, an impedance minimum of 65 Ω occured and a peak phase angle of 61° was reached (Table 2, Fig. 5a), resulting in a velocity amplitude of 7.9 m/s and a displacement amplitude of 25.3 μm_p at an electrical power of 10.2 W.

3.3. Cutting ability

The cutting ability depends mainly on the mechanical performance of the scalpel, related to the achievable velocity amplitude, and the shape of the tip. All prototypes featured the same tip design, except for AD295-pe and AD295-se. Table 2 lists the mean measurements of the standardized test specifying the time required for a scalpel prototype to

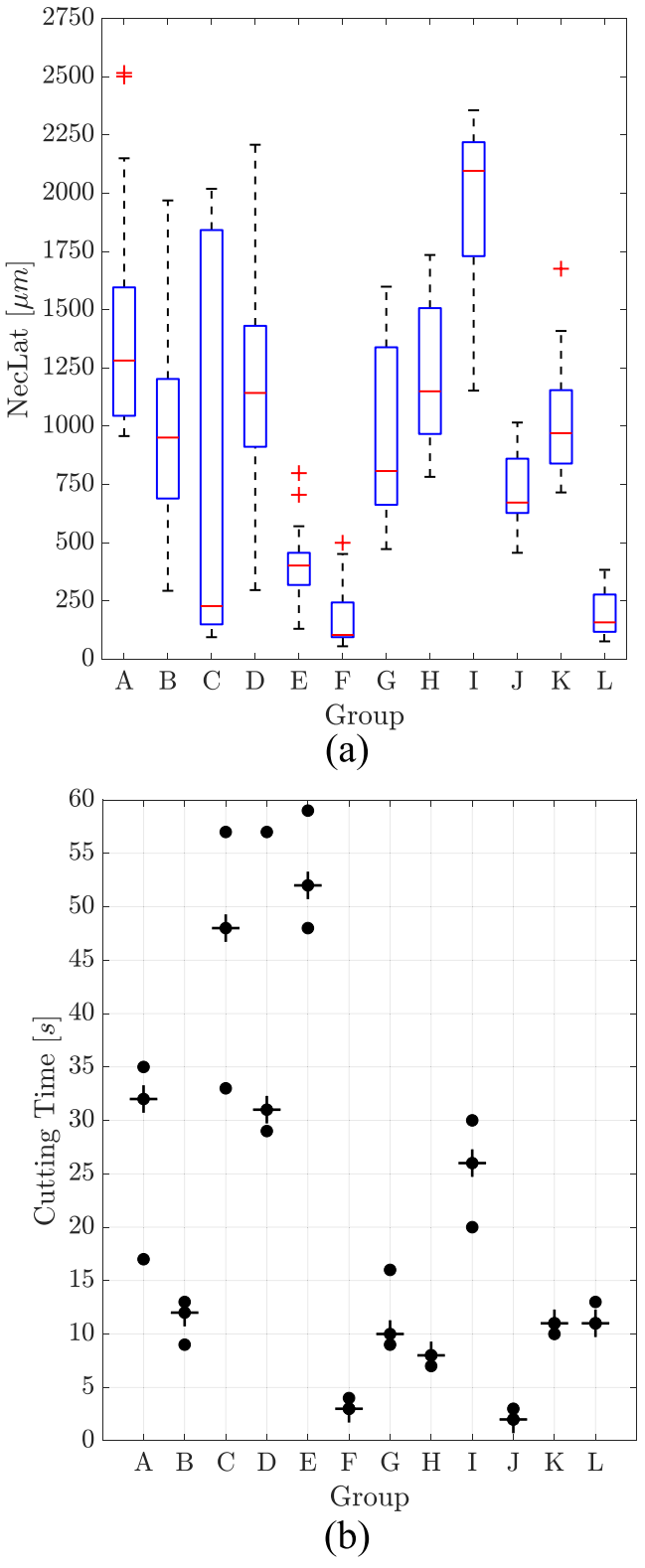

Fig. 6. (a) Examination of the lateral necrosis for groups A to L with n = 18 measurements per group; (b) required cutting time for n = 3 incisions per group (median: +).

penetrate the synthetic muscle tissue sample. Four measurements were performed with two different tissue thicknesses (5 and 10 mm) at matched and unmatched resonance for n = 3 samples per prototype. Operation at the unmatched resonance required less time and offered better cutting performance. Furthermore, most prototypes were unable to perform 10 mm cuts when operating in matched resonance, indicating that this mode is more sensitive to lateral tip contact. The adhesive AD295 offered the best results among the epoxy adhesives and the soldered prototypes showed comparable values to the adhesively bonded ones. Best cutting ability was achieved with the pointed tip shape. These findings were also confirmed by the cutting tests in the animal experiment (Table 3, Fig. 6b).

3.4. Histological examination

All histologically assessed muscular and dermal scalpel-induced incisions were found to present a certain degree of coagulative tissue necrosis (Table 3, Fig. 6a). The extent of necrosis varied between and within the different groups ($p < 0.001$), the type of instrument ($p < 0.001$), and tissue type ($p = 0.009$). The mean extent of incision-induced necrosis was highest in group I (AD295-pe, 48 kHz, skin tissue) and lowest in group F (Electro Cautery, muscle tissue). A microphotograph of an H&E-stained cross-section of the incision performed with prototype AD295-pe in muscle and skin tissue is shown in Fig. 7. When comparing the different scalpel types, the necrotic changes in muscular tissue were most severe in incisions caused by the AD295-pe, 48 kHz scalpel, group A (median lateral necrosis of 1282 µm, IQR 511 µm) and only mild in the standard steel scalpel induced incisions, group L (median lateral necrosis of 159 µm, IQR 160 µm). Median values of necrosis were higher in skin (997 µm, IQR 1061 µm) compared to muscle (794 µm, IQR 958 µm) tissue. Inflammatory changes were either absent (groups B, D, F, H, I, J, K) or minimal (groups A, C, E, G, L). In the microscalpel-induced incisions (groups A, C, E), the observed inflammation was considered to be associated with the scalpel-induced (or other surgically induced) lesions, which was present in 5 out of 9 examined incisions. The inflammation was mild, predominantly neutrophilic, and perivascular. A similar inflammatory change was observed in one out of three standard steel scalpel-induced incisions (group L). Other potentially relevant acute incision-associated effects (i.e. hemorrhage, edema) were not observed. Due to the given timing, tissue sampling was performed 3 h after incisions, the presence of more chronic pathological lesions and the wound healing process could not be assessed. The cutting time required for individual incisions and histological measurements of muscle and skin necrosis are provided in Table 6.

4. Summary and discussion

Seven prototypes were produced and examined for their performance. The resonant frequencies were in the expected range with less than 1 kHz deviation. The only exception was AD295-pe, which had an increased resonant frequency of 50.2 kHz in unmatched mode, due to reduced material at the tapered tip. These similarities indicate a good reproducibility of the prototype fabrication. However, due to cost and time constraints, only one prototype was produced for a specific configuration. Therefore, no statistical values could be obtained for the manufacturing process.

The FE model created for the AD295 configurations was consistent with the unmatched mode. The model allows further refinement of the transducer and tip design. The simulation was adapted to the electrical impedance amplitude at low power. The impedance values agreed well with the measurements for different configurations (Fig. 8). The same applied to the resonance frequencies, deviating from measurements by less than 1 % for the designs st and pe and by a maximum of 2.3 % for AD295-se (Fig. 8, Table 2). For the unmatched mode, simulated vibration amplitudes were in the range of the measured values. However, measurements in matched mode at higher power showed strong nonlinear behaviour, requiring further improvement of the electromechanical coupling in the simulation.

For all prototypes, the A_{31}^{-1} factor in matched mode was only about half of that for unmatched mode. It can be concluded that the

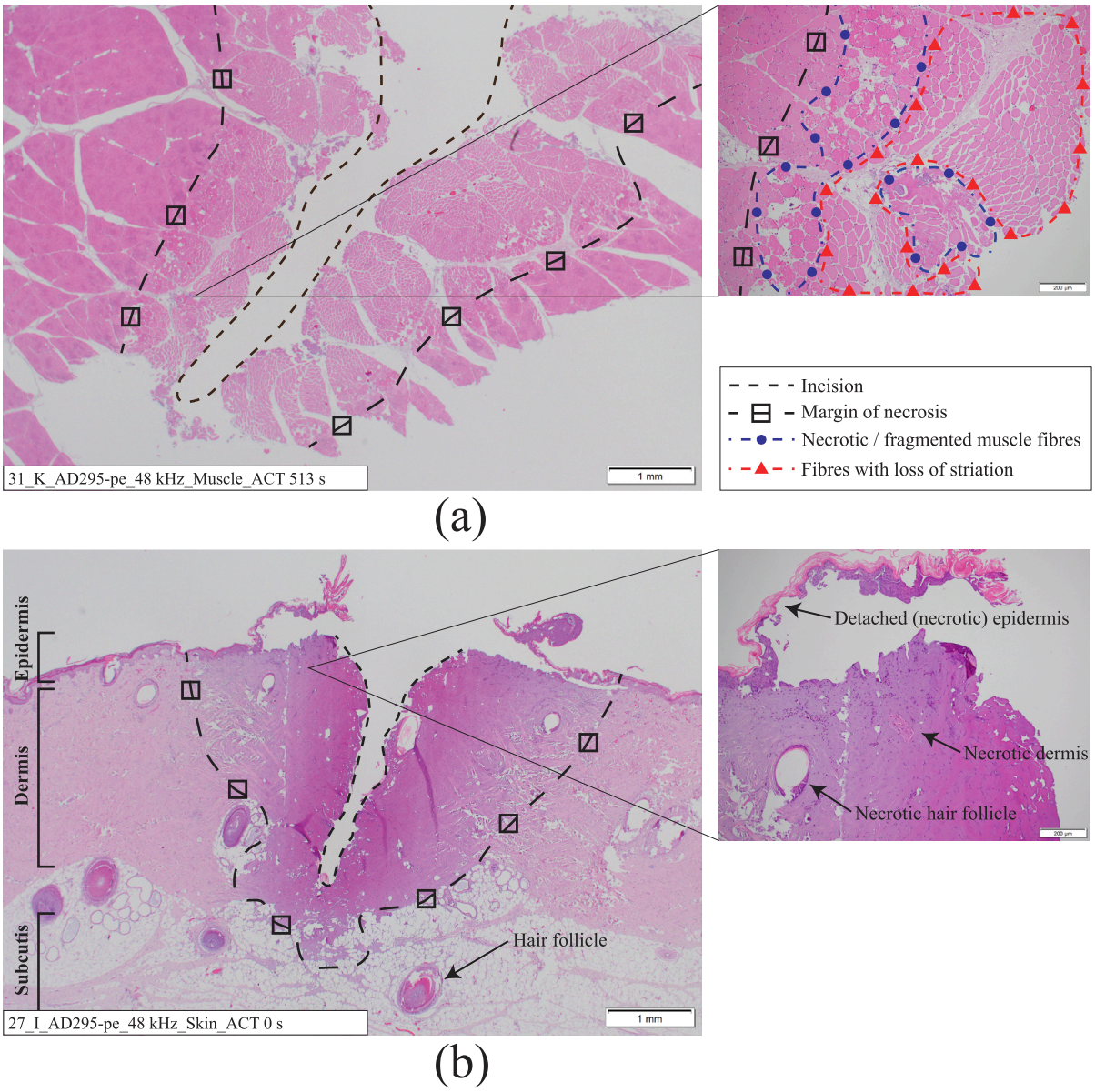

Fig. 7. Histological examination of cross-sections of incisions (H&E-stained) performed with prototype AD295-pe operated in the unmatched mode for (a) muscle tissue with heparin supplementation (ACT: 513 s) and (b) skin tissue.

unmatched λ mode is more suitable for operation. This supposition is also confirmed by the cutting test on synthetic tissue and in the animal experiment. In addition, the match mode has stronger hysteresis, a lower quality factor, and occurring stresses in the piezoceramics are believed to be higher. Compared to previous findings [18], these results are consistent, but it could not be confirmed that the matched mode is more resistant to external loads. All prototypes achieved the required minimum displacement of 15 μm_p [19] (4.5 m/s at 48 kHz) in unmatched mode operation (Fig. 5a). The prototypes with low-temperature solder paste (#281, #SN62) had similar characteristics to the adhesively bonded scalpels and did not offer any significant advantages. Although soldering would allow the use of narrower PZT plates, as no lateral contacting of the electrodes is required, it was more difficult to position the piezoceramics during the reflow process because of the liquefying solder. This issue was observed with prototype #281-st, where the two piezo plates were offset by 1.3 mm in the longitudinal direction, resulting in low parasitic resonances at 39.5 kHz and 47.75 kHz near the target resonances (Fig. 5a). A comparison of the adhesives showed that GE785-st provide the highest Q_m and lowest Z_r values, for both matched and unmatched mode, while A_{31}^{-1} was not significantly affected. It should be mentioned that the quality factor is power dependent and the 3 dB method can only be used to a limited extent, especially for the hysteresis-affected matched mode. Determining Q_m with the electrical transient method would be more appropriate [34,35]. Although the tip modification on the AD295-pe prototype appeared to reduce the quality factor, it offered the highest A_{31}^{-1} factor and best cutting ability in the standardized test (5 mm: 1.1 s and 10 mm: 1.8 s). AD295-pe was therefore chosen for the additional cutting tests in the animal experiment (skin incisions, reduced blood clotting). The higher velocity of the AD295-pe in unmatched operation resulted from maintaining a comparable displacement amplitude to the other AD295 prototypes while having an increased resonant frequency. Further, the pointy tip design facilitated the penetration of the tissue and thus increased the cutting efficiency. The side-edged tip shape (AD295-se) did not have any benefits. In addition, a shift to lower frequencies was observed, which does not agree with theory and simulation. This shift likely resulted from manufacturing tolerances with a longer PZT plate (38.95 mm) and increased bonding layer thickness (230 μm). In monitoring the

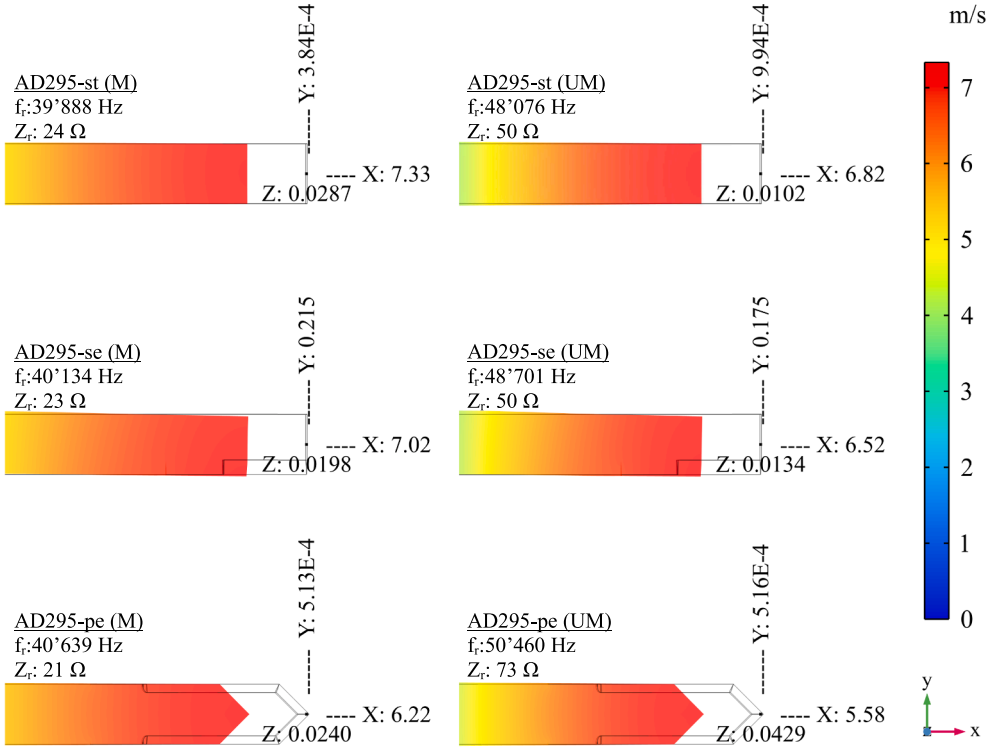

Fig. 8. Analysis of tip mode using FE simulation. Achievable velocity components in X, Y, Z direction of the tip extremity for the three tip designs (st, se, pe) at an operating voltage of 20 V_p for both matched (M) and unmatched (UM) mode. Additional information about corresponding resonant frequencies and impedance values.

temperature of the AD066-st prototype under extreme conditions, steady state was not reached (Fig. 9b). However, it can be assumed that the heating caused mainly by friction at the tip is below 60 °C, which is consistent with previous research [18] and should not pose any substantial risk to the adhesive or the PZT plates. In further development, a temperature measurement should be carried out during soft tissue cutting, since a lower heating is expected. In addition, cyclic operational tests should be conducted to evaluate the longevity of the transducers. The operating power was limited by the maximum amplifier's current (450 mA). Although the inverse force factor remained constant within the limits of the measured power (Fig. 5b), the behaviour at higher power should also be investigated. Higher vibration amplitudes comparable to commercial devices (9–25 m/s) [8] could be achieved. However, generated heat and stress limit the power output, as material failure of the non-prestressed piezoceramics and the adhesive may occur. Adding flanges to the position of the node on the titanium horn is likely to improve the transducer fixation and reduce the stress in the PZT. In comparison to previous research, the microscalpel (AD295-pe) has a velocity amplitude (7.9 m/s, 25 μm_p, 50.2 kHz, 30 V_p) similar to those of the silicon-based prototypes (8.5 m/s, 18 μm_p, 76 kHz, 35 V_p) [18], but achieves a higher displacement amplitude and operates at a lower frequency, making it more comparable to commercial devices (47–55 kHz). Compared to the most powerful miniaturized Langevin transducer (BLT4-stepped, 1.4 m/s, 5 μm_p, 44 kHz, 30 V_p) [19], the AD295-pe has a similar resonant frequency but achieves a considerably higher mechanical vibration amplitude at the same operating voltage. Although the titanium-based planar design is slightly larger than the compared miniaturized systems, the width could be reduced without significantly changing the resonant frequency.

In the animal experiment, all incisions, except those performed with the standard steel scalpel, showed a rapid coagulation effect (<1 s), even with heparin supplementation. This confirms the ability of the novel microscalpel design to cut and coagulate soft tissue. In comparison to commercially available devices, the microscalpel prototypes (except group K) caused slightly more necrotic changes and were slower in cutting (Table 3). It should be noted that the cutting time is highly dependent on the force applied and the surgeon's practice, which would explain the significant difference between group A: 32 (9) s and K: 11 (0.5) s. It is also apparent that the prototypes are less suitable, as ultrasonic instruments in general, for skin incisions. The limited cutting ability of the prototypes is mainly due to the use of a non-optimally tuned electrical controller and the less sophisticated tip geometry. Compared to ultrasonic devices, electrosurgery had a higher smoke generation but was faster in cutting and coagulating muscle tissue and caused less tissue necrosis. Furthermore, precise work was more restricted because the muscle contracts and twitches due to the electric current flow. The results on tissue lesions are not in agreement with other studies [14,16]. However, the tissue was explanted after 3 h for histological analysis and there is insufficient information on the prolonged healing process.

5. Conclusion

A planar d_{31} mode titanium-based ultrasonic scalpel design was devised and fabricated that is smaller than commercial devices and operates in a similar frequency range. Its use for cutting and coagulating soft tissue has been verified. Various bonding materials and tip designs were investigated for their cutting efficiency. The tip geometry had a major effect on the cutting performance and may be further improved. The elaborated design also allows further miniaturization. The design of the amplification part was kept the same for all prototypes and provided good results in terms of amplification factor of the vibration and occurring stresses. However, this section could be further optimized to achieve higher vibration amplitudes. The most suitable configuration is based on the epoxy adhesive Delo Monopox AD295 and has a pointy-edged tip. Operation in the unmatched λ mode at around 48 kHz is

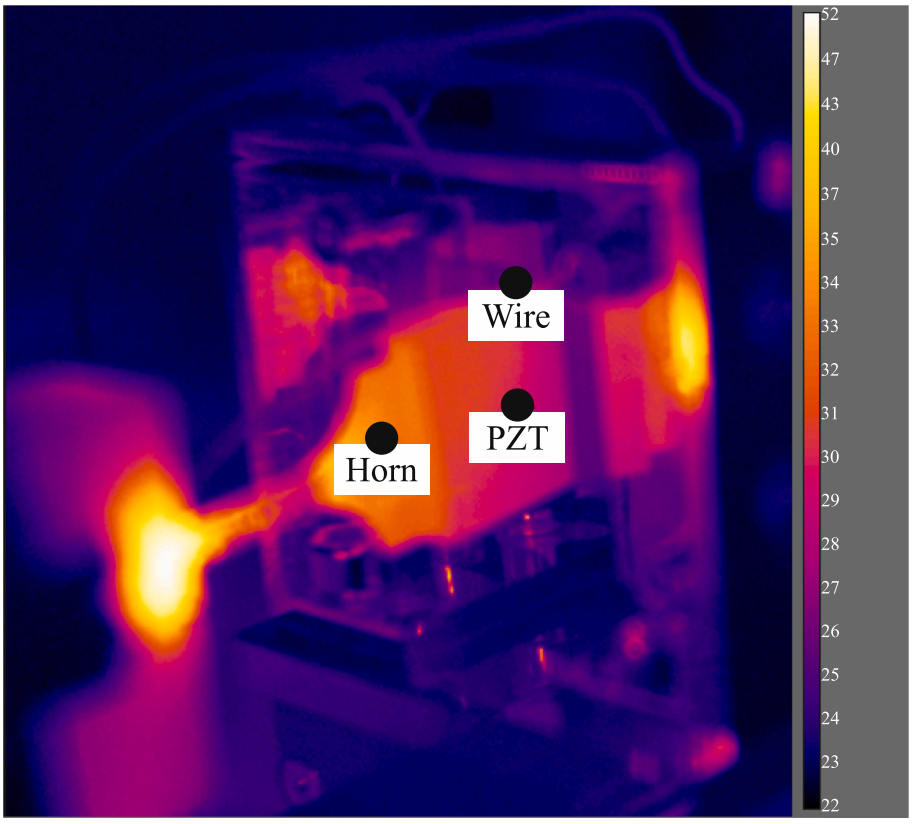

(a)

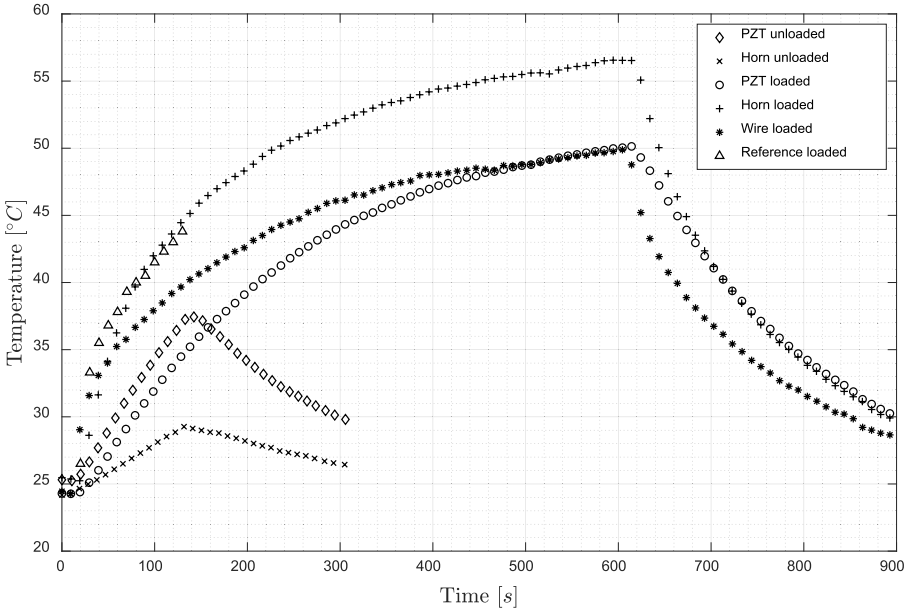

(b)

Fig. 9. (a) Thermographic measurements of heat development; (b) unloaded operation for 120 s followed by a cooling phase. Additional long-term measurement of 10 min in an extreme loaded condition with a PTFE block applying a force of 1.5 N to the tip. Both measurements were performed with the prototype AD066-st operated at unmatched resonance using the GEN 300 generator at maximum power level. Measurement data of the reference thermocouple for loaded operation are limited to the first 2 min.

recommended, as higher vibration amplitudes and thus better cutting ability have been achieved. For further improvements, the focus should be on developing a tuned controller and power amplifier to operate the microscalpel optimally.

Funding

This research did not receive any specific grant from funding agencies in the public, commercial, or not-for-profit sectors.

CRediT authorship contribution statement

Martin Hofmann: Conceptualization, Methodology, Investigation, Formal analysis, Visualization, Writing – original draft. **Andreas Haeberlin:** Investigation, Resources, Writing – review & editing. **Simone de Brot:** Investigation, Formal analysis, Writing – review & editing. **Andreas Stahel:** Conceptualization, Supervision. **Herbert Keppner:** Conceptualization, Resources. **Juergen Burger:** Conceptualization, Supervision, Project administration, Writing – review & editing.

Declaration of Competing Interest

The authors declare that they have no known competing financial interests or personal relationships that could have appeared to influence the work reported in this paper.

Data availability

Data will be made available on request.

Appendix

Table 4
Comparison of suitable horn materials for planar ultrasonic transducers with measurements of the used titanium alloy Ti64 and reference material properties of medical grade stainless steel 316 LVM [36], aluminium alloy AL7075-T6 [37], and monocrystalline silicon (1 0 0) Si [20,38,39]. Speed of sound $c = \sqrt{E/\rho}$ [a)]Calculation based on mean value.

	Ti64	316 LVM	Al7075-T6	Si
Composition	Ti6Al4V	Fe18Cr14Ni2.5Mo	AlZn5.5MgCu	Si (1 0 0) ⟨1 1 0⟩
Density ρ [kg/m^3]	4450	8030	2810	2330
Young's modulus E [GPa]	114	192–201	72	169
Tensile Strength σ_{max} [MPa]	1080	496–1340	570	6900
Poisson ratio v	0.34	0.265–0.275	0.33	0.28
Speed of sound c [m/s]	5061	4947[a)]	5062	8517

Table 5
Material properties of the different one-component epoxy adhesives (DELO Industrie Klebstoffe GmbH & Co., Germany) and solder paste (Indium corp., United States) used. The specifications were taken from the corresponding data sheets. N/A: not available.

	DELO Monopox AD066	DELO Monopox AD295	DELO Monopox GE785	Indalloy #281	Indalloy #Sn62
Composition	N/A	N/A	N/A	58Bi42Sn	62Sn36Pb2Ag
Density ρ [kg/m^3]	1200	1600	1740	8560	8410
Young's modulus E [GPa]	2.9	5.5	11	N/A	N/A
Tensile Strength σ_{max} [MPa]	45	50	55	55.2	48.3
Viscosity [Pa·s]	20	230	135	200	200
Glass transition temp. T_g [C]	132	134	182	N/A	N/A
Melting point T_m [C]	N/A	N/A	N/A	138	179

Table 6
Required cutting time and histological measurements of muscle and skin necrosis at the incision site, indicated for each of the grouped incisions.

ID	Group	Scalpel type	Frequency	Tissue	ACT	Cut Time	CrossA1	CrossA2	CrossA3	CrossB1	CrossB2	CrossB3	Median Group	IQR Group
			[kHz]		[s]	[s]	[µm]	[µm]	[µm]	[µm]	[µm]	[µm]	[µm]	[µm]
1	A	AD295-pe	48	Muscle	0	35	1197	958	1023	1032	1043	1551	1282	551
2	A	AD295-pe	48	Muscle	0	32	1284	1503	1280	2150	1945	1045		
3	A	AD295-pe	48	Muscle	0	17	2501	2516	1191	1207	1567	1596		
4	B	Harmonic Synergy (Syn)	55	Muscle	0	13	863	1203	953	423	708	785	952	513
5	B	Harmonic Synergy (Syn)	55	Muscle	0	12	1488	1424	690	950	1101	990		
6[a)]	B	Harmonic Synergy (Syn)	55	Muscle	0	9	1969	1365	1095	630	448	294		
7[b)]	C	AD295-st	48	Muscle	0	33	212	266	150	156	196	137	229	1692
8[c)]	C	AD295-st	48	Muscle	0	57	245	346	145	171	142	95		
9	C	AD295-st	48	Muscle	0	48	2000	1830	1899	1842	1888	2019		
10	D	AD295-se	48	Muscle	0	57	1591	1640	1139	2096	2208	1431	1143	519
11	D	AD295-se	48	Muscle	0	29	574	1260	1189	508	666	297		
12	D	AD295-se	48	Muscle	0	31	912	1143	1033	935	1143	1351		
13[d)]	E	AD295-pe	40	Muscle	0	52	799	571	543	442	387	231	403	138
14	E	AD295-pe	40	Muscle	0	48	319	215	365	415	457	423		
15	E	AD295-pe	40	Muscle	0	59	219	430	131	706	347	390		
16	F	ErgoPEN (Elec)	350	Muscle	513	3	190	500	452	381	367	244	105	149
17[e)]	F		350	Muscle	513	3	59	75	102	95	56	92		

(continued on next page)

Table 6 (*continued*)

ID	Group	Scalpel type	Frequency	Tissue	ACT	Cut Time	CrossA1	CrossA2	CrossA3	CrossB1	CrossB2	CrossB3	Median Group	IQR Group
		ErgoPEN (Elec)												
18[f)]	F	ErgoPEN (Elec)	350	Muscle	513	3	123	153	101	107	100	98		
19	G	Harmonic Synergy (Syn)	55	Skin	0	16	1495	1436	804	994	1339	1599	808	676
20	G	Harmonic Synergy (Syn)	55	Skin	0	9	812	648	576	473	794	1203		
21	G	Harmonic Synergy (Syn)	55	Skin	0	10	1541	679	480	1240	769	663		
22	H	Harmonic Synergy (Syn)	55	Muscle	513	7	1652	1598	1520	1261	1205	788	1150	540
23	H	Harmonic Synergy (Syn)	55	Muscle	513	8	1090	1077	960	1231	1193	1047		
24	H	Harmonic Synergy (Syn)	55	Muscle	513	8	967	879	783	1735	1507	1107		
25	I	AD295-pe	48	Skin	0	30	2097	2095	1639	2219	2325	1917	2096	489
26	I	AD295-pe	48	Skin	0	26	1730	1492	1153	2128	2052	1996		
27	I	AD295-pe	48	Skin	0	20	2203	2142	1225	2356	2259	2272		
28	J	ErgoPEN	350	Skin	0	2	655	999	676	655	613	606	673	233
29	J	ErgoPEN	350	Skin	0	2	1016	956	628	861	989	628		
30	J	ErgoPEN	350	Skin	0	2	711	747	457	755	669	553		
31	K	AD295-pe	48	Muscle	513	10	1409	1155	1013	993	1676	1345	971	315
32	K	AD295-pe	48	Muscle	513	11	1062	941	904	868	948	749		
33	K	AD295-pe	48	Muscle	513	11	716	824	767	1044	1230	840		
34	L	Standard Steel (Stan)	0	Muscle	0	13	349	355	278	216	154	384	159	160
35[g)]	L	Standard Steel (Stan)	0	Muscle	0	11	133	163	130	118	121	173		
36[g)]	L	Standard Steel (Stan)	0	Muscle	0	11	221	278	89	107	88	77		

References

[1] T. Kinoshita, E. Kanehira, K. Omura, K. Kawakami, Y. Watanabe, Experimental study on heat production by a 23.5-kHz ultrasonically activated device for endoscopic surgery, Surg. Endosc. 13 (1999) 621–625, https://doi.org/10.1007/s004649901055.

[2] K.M. Kadesky, B. Schopf, J.F. Magee, G.K. Blair, Proximity injury by the ultrasonically activated scalpel during dissection, J. Pediatr. Surg. 32 (1997) 878–879, https://doi.org/10.1016/S0022-3468(97)90641-2.

[3] C. Power, D. Maguire, O.J. McAnena, J. Calleary, Use of the ultrasonic dissecting scalpel in laparoscopic cholecystectomy, Surg. Endosc. 14 (2000) 1070–1073, https://doi.org/10.1007/s004640000034.

[4] S. Zhang, Y. Guo, Z. Chen, G. Li, Q. Guo, Y. Wu, J. Zeng, Proposal for a novel elliptical ultrasonic aspirator and its fundamental performance in cartilage removal, Ultrasonics. 109 (2021), 106259, https://doi.org/10.1016/j.ultras.2020.106259.

[5] B.J. O'Daly, E. Morris, G.P. Gavin, J.M. O'Byrne, G.B. McGuinness, High-power low-frequency ultrasound: A review of tissue dissection and ablation in medicine and surgery, J. Mater. Process. Technol. 200 (2008) 38–58, https://doi.org/10.1016/j.jmatprotec.2007.11.041.

[6] F. Bejarano, A. Feeney, R. Wallace, H. Simpson, M. Lucas, An ultrasonic orthopaedic surgical device based on a cymbal transducer, Ultrasonics. 72 (2016) 24–33, https://doi.org/10.1016/j.ultras.2016.07.004.

[7] K. Ebina, H. Hasegawa, H. Kanai, Investigation of frequency characteristics in cutting of soft tissue using prototype ultrasonic knives, Japanese J. Appl. Physics, Part 1 Regul. Pap. Short Notes Rev. Pap. 46 (2007) 4793–4800, https://doi.org/10.1143/JJAP.46.4793.

[8] W.W. Cimino, The physics of soft tissue fragmentation using ultrasonic frequency vibration of metal probes, Clin. Plast. Surg. 26 (1999) 447–461, https://doi.org/10.1016/s0094-1298(20)32638-9.

[9] M. Lucas, A. Mathieson, Ultrasonic cutting for surgical applications, in: J. A. Gallego-Juárez, K.F. Graff (Eds.), Power Ultrason, Woodhead Publishing, Oxford, 2015, pp. 695–721, https://doi.org/10.1016/B978-1-78242-028-6.00023-5.

[10] W.W. Cimino, L.J. Bond, Physics of ultrasonic surgery using tissue fragmentation: Part I, Ultrasound Med. Biol. 22 (1996) 89–100, https://doi.org/10.1016/0301-5629(95)02021-7.

[11] D. Gossot, G. Buess, A. Cuschieri, E. Leporte, M. Lirici, R. Marvik, D. Meijer, A. Melzer, M.O. Schurr, Ultrasonic dissection for endoscopic surgery, Surg. Endosc. 13 (1999) 412–417, https://doi.org/10.1007/s004649901002.

[12] M.E. Schafer, 21 - Ultrasonic surgical devices and procedures, in: J.A. Gallego-Juárez, K.F. Graff (Eds.), Power Ultrason, Woodhead Publishing, Oxford, 2015, pp. 633–660, https://doi.org/10.1016/B978-1-78242-028-6.00021-1.

[13] S. Deo, S. Hazarika, N.K. Shukla, M. Kar, A. Samaiya, A prospective randomized trial comparing harmonic scalpel versus electrocautery for pectoralis major myocutaneous flap dissection, Plast. Reconstr. Surg. 115 (2005) 1006–1009, https://doi.org/10.1097/01.PRS.0000154209.21728.51.

[14] H. Inaba, Y. Kaneko, T. Ohtsuka, M. Ezure, K. Tanaka, K. Ueno, S. Takamoto, Minimal damage during endoscopic latissimus dorsi muscle mobilization with the harmonic scalpel, Ann. Thorac. Surg. 69 (2000) 1399–1401, https://doi.org/10.1016/S0003-4975(00)01136-X.

[15] R.P.G. Ten Broek, J. Wilbers, H. Van Goor, Electrocautery causes more ischemic peritoneal tissue damage than ultrasonic dissection, Surg. Endosc. 25 (2011) 1827–1834, https://doi.org/10.1007/s00464-010-1474-3.

[16] T. Diamantis, M. Kontos, A. Arvelakis, S. Syroukis, D. Koronarchis, A. Papalois, E. Agapitos, E. Bastounis, A.C. Lazaris, Comparison of monopolar electrocoagulation, bipolar electrocoagulation, ultracision, and ligasure, Surg. Today. 36 (2006) 908–913, https://doi.org/10.1007/s00595-006-3254-1.

[17] D.N. Armstrong, W.L. Ambroze, M.E. Schertzer, G.R. Orangio, Harmonic Scalpel® vs. electrocautery hemorrhoidectomy: A prospective evaluation, Dis. Colon Rectum. 44 (2001) 558–564, https://doi.org/10.1007/BF02234329.

[18] R. Lockhart, F. Friedrich, D. Briand, P. Margairaz, J.P. Sandoz, J. Brossard, H. Keppner, W. Olson, T. Dietz, Y. Tardy, H. Meyer, P. Stadelmann, C. Robert, A. Boegli, P.A. Farine, N.F. de Rooij, J. Burger, Silicon micromachined ultrasonic scalpel for the dissection and coagulation of tissue, Biomed. Microdevices. 17 (2015) 1–12, https://doi.org/10.1007/s10544-015-9981-6.

[19] X. Li, T. Stritch, K. Manley, M. Lucas, Limits and Opportunities for Miniaturizing Ultrasonic Surgical Devices Based on a Langevin Transducer, IEEE Trans. Ultrason. Ferroelectr. Freq. Control. 68 (2021) 2543–2553, https://doi.org/10.1109/TUFFC.2021.3065207.

[20] A. Lal, R.M. White, Silicon microfabricated horns for power ultrasonics, Int. Conf. Solid-State Sensors Actuators, Eurosensors IX, Proc. 1 (1995) 405–408, https://doi.org/10.1109/sensor.1995.717221.

[21] A. Lal, R.M. White, Silicon micromachined ultrasonic micro-cutter, Proc. IEEE Ultrason. Symp. 3 (1994) 1907–1911, https://doi.org/10.1109/ultsym.1994.401964.

[22] X. Lu, J. Hu, H. Peng, Y. Wang, A new topological structure for the Langevin-type ultrasonic transducer, Ultrasonics. 75 (2017) 1–8, https://doi.org/10.1016/j.ultras.2016.11.008.

[23] K. Uchino, Piezoelectric ceramics for transducers, Woodhead Publishing Limited (2012), https://doi.org/10.1533/9780857096302.1.70.

[24] D.A. Wang, H.D. Nguyen, A planar Bézier profiled horn for reducing penetration force in ultrasonic cutting, Ultrasonics. 54 (2014) 375–384, https://doi.org/10.1016/j.ultras.2013.05.002.

[25] M.R. Sadiq, Y. Kuang, Z. Huang, S. Cochran, Ultrasonic cutting with a d 31-mode PMN-PT-driven planar tool, IEEE Int. Ultrason. Symp. IUS. (2011) 2189–2192, https://doi.org/10.1109/ULTSYM.2011.0543.

[26] A. Cardoni, A. MacBeath, M. Lucas, Methods for reducing cutting temperature in ultrasonic cutting of bone, Ultrasonics. 44 (2006) 37–42, https://doi.org/10.1016/j.ultras.2006.06.046.

[27] L. Lebrun, G. Sebald, B. Guiffard, C. Richard, D. Guyomar, E. Pleska, Investigations on ferroelectric PMN-PT and PZN-PT single crystals ability for power or resonant actuators, Ultrasonics. 42 (2004) 501–505, https://doi.org/10.1016/j.ultras.2004.01.028.
[28] S.R. Anton, A. Erturk, D.J. Inman, Bending strength of piezoelectric ceramics and single crystals for multifunctional load-bearing applications, IEEE Trans. Ultrason. Ferroelectr. Freq. Control. 59 (2012) 1085–1092, https://doi.org/10.1109/TUFFC.2012.2299.
[29] D.M. Brunette, P. Tengvall, M. Textor, P. Thomsen, Titanium in Medicine : material science, surface science, engineering, biological responses and medical applications, Springer, Berlin Heidelberg, Berlin, Heidelberg (2001), https://doi.org/10.1007/978-3-642-56486-4.
[30] H. Shekhani, T. Scholehwar, E. Hennig, K. Uchino, Characterization of piezoelectric ceramics using the burst/transient method with resonance and antiresonance analysis, J. Am. Ceram. Soc. 100 (2017) 998–1010, https://doi.org/10.1111/jace.14580.
[31] S. Albert, C. Guedon, C. Halimi, J.P. Cristofari, B. Barry, The Use of Harmonic Scalpel for Free Flap Dissection in Head and Neck Reconstructive Surgery, Plast. Surg. Int. 2012 (2012) 1–4, https://doi.org/10.1155/2012/302921.
[32] J.J. Vaitekunas, F.B. Stulen, E.S. Grood, Effects of Frequency on the Cutting Ability of an Ultrasonic Surgical Instrument, Ultrason. Ind. Assoc Symp. (2001).
[33] Y. Kubo, K. Yamashita, T. Saito, K. Tanaka, T. Makino, T. Takahashi, Y. Kurokawa, M. Yamasaki, H. Eguchi, Y. Doki, K. Nakajima, Heparinized swine models for better surgical/endoscopic training, DEN Open. 2 (2022) 1–6, https://doi.org/10.1002/deo2.64.
[34] K. Nakamura, Ultrasonic transducers: Materials and design for sensors, actuators and medical applications, Woodhead Publishing Limited (2012), https://doi.org/10.1533/9780857096302.
[35] M. Umeda, K. Nakamura, S. Ueha, The measurement of high-power characteristics for a piezoelectric transducer based on the electrical transient response, Japanese J. Appl. Physics, Part 1 Regul. Pap. Short Notes Rev. Pap. 37 (1998) 5322–5325, https://doi.org/10.1143/jjap.37.5322.
[36] ASM, ASM Handbook Volume 23, Materials for Medical Devices, 2012.
[37] ASM, ASM Handbook Volume 2, Properties and Selection: Nonferrous Alloys and Special-Purpose Materials, 1990.
[38] K.E. Petersen, Silicon as a mechanical material, Micromech. MEMS Class. Semin. Pap. To 1990 70 (1997) 58–95, https://doi.org/10.1109/9780470545263.sect1.
[39] M.A. Hopcroft, W.D. Nix, T.W. Kenny, What is the Young's modulus of silicon? J. Microelectromech. Syst. 19 (2010) 229–238, https://doi.org/10.1109/JMEMS.2009.2039697.